Atoms-in-Molecules Dual Parameter Analysis of Weak to Strong Interactions: Behaviors of Electronic Energy Densities versus Laplacian of Electron Densities at Bond Critical Points

Waro Nakanishi,* Satoko Hayashi, and Kenji Narahara

Department of Material Science and Chemistry, Faculty of Systems Engineering, Wakayama University, 930 Sakaedani, Wakayama, 640-8510 Japan

Received: June 21, 2008; Revised Manuscript Received: October 9, 2008

AIM dual parameter analysis is proposed for the better understanding of weak to strong interactions: Total electron energy densities ($H_b(\boldsymbol{r}_c)$) are plotted versus Laplacian of electron densities ($\Delta\rho_b(\boldsymbol{r}_c)$) at bond critical points (BCPs). Interactions examined in this work are those in van der Waals adducts, hydrogen bonded complexes, molecular complexes and hypervalent adducts through charge transfer (CT) interactions, and some classical covalent bonds. Data calculated at BCPs for the optimized distances (r_o), together with $r_o - 0.1$ Å, $r_o + 0.1$ Å, and $r_o + 0.2$ Å, are employed for the plots. The plots of $H_b(\boldsymbol{r}_c)$ versus $\Delta\rho_b(\boldsymbol{r}_c)$ start from near origin ($H_b(\boldsymbol{r}_c) = \Delta\rho_b(\boldsymbol{r}_c) = 0$) and turn to the right drawing a helical stream as a whole. The helical nature is demonstrated to be controlled by the relative magnitudes of kinetic energy densities ($G_b(\boldsymbol{r}_c)$) and potential energy densities ($V_b(\boldsymbol{r}_c)$), where $G_b(\boldsymbol{r}_c) + V_b(\boldsymbol{r}_c) = H_b(\boldsymbol{r}_c)$. Requirements for the data to appear in the specified quadrant are clarified. Points corresponding to the data will appear in the first quadrant ($\Delta\rho_b(\boldsymbol{r}_c) > 0$ and $H_b(\boldsymbol{r}_c) > 0$) when $-V_b(\boldsymbol{r}_c) < G_b(\boldsymbol{r}_c)$, they drop in the forth one ($\Delta\rho_b(\boldsymbol{r}_c) > 0$ and $H_b(\boldsymbol{r}_c) < 0$) if $-(1/2)V_b(\boldsymbol{r}_c) < G_b(\boldsymbol{r}_c) < -V_b(\boldsymbol{r}_c)$, and they appear in the third quadrant ($\Delta\rho_b(\boldsymbol{r}_c) < 0$ and $H_b(\boldsymbol{r}_c) < 0$) when $G_b(\boldsymbol{r}_c) < -(1/2)V_b(\boldsymbol{r}_c)$. No points will appear in the second quadrant ($\Delta\rho_b(\boldsymbol{r}_c) < 0$ and $H_b(\boldsymbol{r}_c) > 0$). The physical meanings of the plots proposed in this work are also considered. The helical nature of the interactions in the plots helps us to understand the interactions in a unified way.

Introduction

Weak interactions are of current interest[1−11] since they determine fine structures of compounds and create high functionalities of materials, whereas strong bonds such as classical covalent bonds set up the skeleton of molecules. Weak interactions play an important role in physical, chemical, and biological sciences, such as in the crystal engineering for material development,[12] donor−acceptor complexes for electronic materials,[13] supermolecular chemistry,[14] and stabilization and activity of biological materials.[15,16] Investigations successfully utilizing weak interactions are increasing; however, it is still of high importance to clarify the cause-and-effect in the phenomena arising from weak interactions with physical necessity. We searched for the method to evaluate and classify weak interactions, together with strong interactions, for better understanding the interactions.

Bader proposed the atoms-in-molecules method (AIM),[17−19] which enables us to analyze the nature of chemical bonds and interactions.[20−25] Some criteria have been proposed to analyze chemical bonds and interactions based on AIM parameters at bond critical points (BCPs: $\boldsymbol{r}_c$).[17,18] Electron densities at BCPs ($\rho_b(\boldsymbol{r}_c)$) are strongly correlated to the binding energies for several types of bonding interactions.[26−33] The bond order (BO) corresponds to the strength of a chemical bond: BO is correlated to $\rho_b(\boldsymbol{r}_c)$ by $\mathrm{BO} = \exp[A(\rho_b(\boldsymbol{r}_c) - B)]$, where A and B are constants which depend on the nature of the bonded atoms.[18] $\rho_b(\boldsymbol{r}_c)$ are shown to be larger than 0.20 a.u. in shared-shell bondings and less than 0.10 a.u. in closed-shell interactions for typical cases.[18]

SCHEME 1: Behaviors of Some AIM Functions at BCPs: $\rho_b(\boldsymbol{r}_c)$, $\Delta\rho_b(\boldsymbol{r}_c)$, and $H_b(\boldsymbol{r}_c)$

Weaker ← Interaction → Stronger		
smaller	$\rho_b(\boldsymbol{r}_c)$	larger
positive	$\Delta\rho_b(\boldsymbol{r}_c)$	negative
positive	$H_b(\boldsymbol{r}_c)$	negative

Laplacian of $\rho_b(\boldsymbol{r}_c)$ ($\Delta\rho_b(\boldsymbol{r}_c)$) is the second derivative of $\rho_b(\boldsymbol{r}_c)$, therefore, the sign indicates that $\rho_b(\boldsymbol{r}_c)$ is depleted or concentrated with respect to the surroundings. The $\rho_b(\boldsymbol{r}_c)$ value is locally depleted relative to the average distribution around $\boldsymbol{r}_c$ when $\Delta\rho_b(\boldsymbol{r}_c) > 0$, but it is concentrated if $\Delta\rho_b(\boldsymbol{r}_c) < 0$. As a general rule, $\Delta\rho_b(\boldsymbol{r}_c)$ are negative for covalent bonds, whereas they become positive when the bonds contain the ionic nature. On the other hand, the total electronic energy densities at BCPs ($H_b(\boldsymbol{r}_c)$) will be a more appropriate index for the weak interactions on the energy basis.[16−18] As shown in eq 1, $H_b(\boldsymbol{r}_c)$ are the sum of the kinetic energy densities ($G_b(\boldsymbol{r}_c)$) and the potential energy densities ($V_b(\boldsymbol{r}_c)$) at BCPs. Equations 2 and 3 represent the relations between $H_b(\boldsymbol{r}_c)$ and $\Delta\rho_b(\boldsymbol{r}_c)$. $H_b(\boldsymbol{r}_c)$ are larger than $(\hbar^2/8m)\Delta\rho_b(\boldsymbol{r}_c)$ by $(1/2)V_b(\boldsymbol{r}_c)$, where $V_b(\boldsymbol{r}_c)$ must be negative at all BCPs. Consequently, $H_b(\boldsymbol{r}_c)$ are negative for covalent bonds with $\Delta\rho_b(\boldsymbol{r}_c) < 0$ whereas $H_b(\boldsymbol{r}_c)$ will be positive for ionic bonds when $\Delta\rho_b(\boldsymbol{r}_c) > 0$, although $(1/2)V_b(\boldsymbol{r}_c)$ must be considered. There should exist some region where $H_b(\boldsymbol{r}_c) < 0$ but $\Delta\rho_b(\boldsymbol{r}_c) > 0$ at BCPs. Scheme 1 summarizes the behavior of the AIM functions. The combined use of the functions will clarify the behaviors of weak to strong interactions. Relative magnitudes of $G_b(\boldsymbol{r}_c)$ and $V_b(\boldsymbol{r}_c)$ would control the behaviors.[33a]

* To whom correspondence should be addressed. E-mail: nakanisi@sys.wakayama-u.ac.jp. Phone: +81-73-457-8252. Fax: +81-73-457-8253.

10.1021/jp8054763 CCC: $40.75
Published on Web 11/24/2008

$$H_b(\boldsymbol{r}_c) = G_b(\boldsymbol{r}_c) + V_b(\boldsymbol{r}_c) \quad (1)$$

$$(\hbar^2/8m)\Delta\rho_b(\boldsymbol{r}_c) = G_b(\boldsymbol{r}_c) + (1/2)V_b(\boldsymbol{r}_c) = H_b(\boldsymbol{r}_c) - (1/2)V_b(\boldsymbol{r}_c) \quad (2)$$

$$H_b(\boldsymbol{r}_c) = (\hbar^2/8m)\Delta\rho_b(\boldsymbol{r}_c) + (1/2)V_b(\boldsymbol{r}_c) \quad (3)$$

We are very interested in extended hypervalent bonds [*m* center−*n* electron bonds (*mc*−*ne*: $m \geq 4$)][2b] higher than 3c−4e. Five C−Z---O---Z−C (Z = O, S, and Se) atoms in 1,8-bis(methylchalcogena)anthraquinones (**A**) and 9-methoxy-1,8-bis(methylchalcogena)anthracenes (**B**) align linearly.[34] The linear C−Z---O---Z−C interactions are analyzed by the extended hypervalent 5c−6e model.[2a] To clarify the nature of the C_2Z_2O 5c−6e, the Z---O interactions are examined based on the AIM parameters at BCPs: $H_b(\boldsymbol{r}_c)$ were plotted versus $\rho_b(\boldsymbol{r}_c)$ for **A** and **B**, together with some weak interactions.[35] The plot was observed to bend at the border area between van der Waals interactions[36] and hydrogen bonds.[37] We wondered if this must show the critical difference between van der Waals interactions and hydrogen bonds.

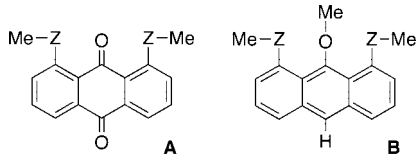

Z = Se (**a**), S (**b**), and O (**c**)

The AIM dual parameter analysis is examined: $H_b(\boldsymbol{r}_c)$ are plotted versus $\Delta\rho_b(\boldsymbol{r}_c)$ for weak to strong interactions after the treatment of $H_b(\boldsymbol{r}_c)$ versus $\rho_b(\boldsymbol{r}_c)$: The treatment of $H_b(\boldsymbol{r}_c)$ versus $\rho_b(\boldsymbol{r}_c)$ is correlated to that of $\Delta\rho_b(\boldsymbol{r}_c)$ versus $\rho_b(\boldsymbol{r}_c)$ by Woźniak.[38] Scheme 2 shows weak to strong interactions examined in this work: van der Waals interactions (vdW), hydrogen bonds (HB), charge transfer (CT) in molecular complexes (CT-MC), and CT in hypervalent trigonal bipyramidal adducts (CT-TBP). Some classical covalent bonds of weak (Cov-w) and strong ones (Cov-s) are also examined. Marks with colors in Scheme 2 correspond to those in the plots. While BCPs in weak interactions are described by --∗--, those in covalent bonds are described as -∗-.

Here, we propose the AIM dual parameter analysis that consists of the plot of $H_b(\boldsymbol{r}_c)$ versus $\Delta\rho_b(\boldsymbol{r}_c)$, for better understanding the weak to strong interactions. Indeed, $H_b(\boldsymbol{r}_c)$ is closely related to $\Delta\rho_b(\boldsymbol{r}_c)$, but the difference between the two must play an important role in the plots. The method will supply a powerful tool to understand, evaluate, and classify the interactions.

Methodological Details. Molecules and adducts in Scheme 2 are optimized employing the 6-311+G(2df,2p) basis sets of the Gaussian 03 program.[39] The 6-311G(2df,2p) basis sets are employed for Ar and Kr and the DGDZVP basis sets for Te and I. The Møller−Plesset second order energy correlation (MP2) level is employed for the calculations.[40]

The X−Y bond lengths (r(X, Y)) in question are optimized to give r_o(X, Y) (=r_o). Optimizations are further performed with the fixed bond lengths r(X, Y) (=r) around the optimized values (r_o), to clarify the trends of interactions.[41,42] The r(X, Y) value is fixed to be shorter than r_o(X, Y) by 0.1 Å and longer than r_o(X, Y) by 0.1 and 0.2 Å for each: r(X, Y) = r_o(X, Y) + 0.1n where n = −1, (0), 1, and 2.[43] Scheme 3 shows BCP ($\boldsymbol{r}_c$, ∗) and the bond lengths (r(X, Y)) employed for the calculations.[42,44]

SCHEME 2: Interactions Examined in This Work[a,b]

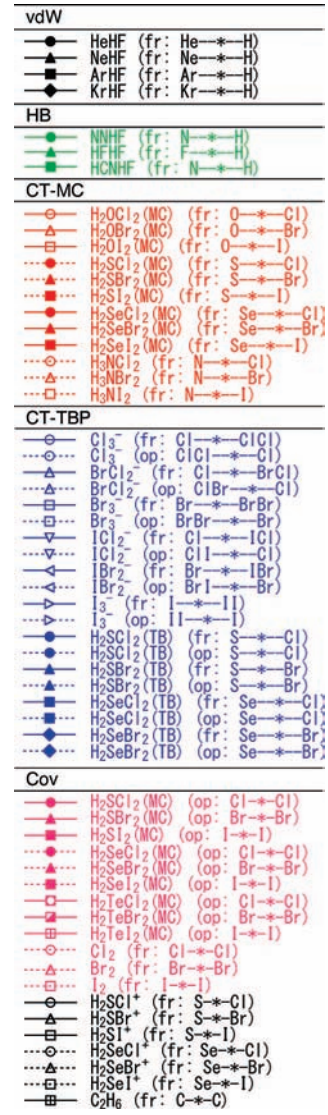

[a] BCPs in weak interactions are described by --∗-- and those in covalent bonds as -∗-. The marks and colors correspond to those in the plots. [b] The fr and op bonds are frozen and optimized at $r = r_o + 0.1n$ Å ($n = \pm 1$ and 2), respectively.

SCHEME 3: Bond Critical Point (BCP, $\boldsymbol{r}_c$, ∗) for Adducts and Molecules with Fixed r(X, Y) Values for Further Optimization Where r_o(X, Y) Are Full Optimized Values

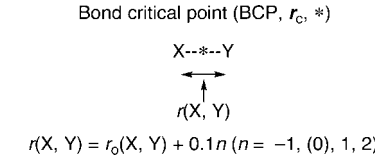

AIM parameters are calculated with the Gaussian 03 program and analyzed employing the AIM2000 program.[45]

Results and Discussion

Table 1 collects AIM parameters, such as r_o(X, Y), $\rho_b(\boldsymbol{r}_c)$, $\Delta\rho_b(\boldsymbol{r}_c)$, $H_b(\boldsymbol{r}_c)$, $G_b(\boldsymbol{r}_c)$, and $V_b(\boldsymbol{r}_c)$, for some typical interactions in Scheme 2, calculated at the MP2 level. The parameters for those containing Te, F, and I are collected in Table S1 of the Supporting Information (SI).

TABLE 1: AIM Parameters for van der Waals Interactions (vdW), Hydrogen Bonds (HB), Molecular Complexes (MC), Trihalide Ions (X_3^-), Chalcogenide Dihalides of TBP Structures (TBP-ZX_2), Together with Weak (Cov-w) and Strong Covalent Bonds (Cov-s)[a]

species	X---Y (BCP)	r_o(X, Y) (Å)	$\rho_b(\boldsymbol{r}_c)$ (ea_0^{-3})	$\Delta\rho_b(\boldsymbol{r}_c)$ (ea_0^{-5})	$H_b(\boldsymbol{r}_c)$ (a.u.)	$G_b(\boldsymbol{r}_c)$ (a.u.)	$V_b(\boldsymbol{r}_c)$ (a.u.)	comment
He---HF[b]	He···H	2.3562	0.0032	0.0143	0.0009	0.0027	−0.0018	vdW
Ne---HF[c]	Ne···H	2.2891	0.0069	0.0338	0.0012	0.0072	−0.0060	vdW
Ar---HF	Ar···H	2.5202	0.0082	0.0341	0.0017	0.0069	−0.0052	vdW
Kr---HF	Kr···H	2.6478	0.0085	0.0307	0.0013	0.0064	−0.0051	vdW
NN---HF[c]	N···H	2.0677	0.0169	0.0647	0.0022	0.0140	−0.0119	HB
HF---HF[c]	F···H	1.8416	0.0234	0.0941	0.0007	0.0228	−0.0221	HB
HCN---HF	N···H	1.8458	0.0308	0.0950	−0.0008	0.0246	−0.0254	HB
H_3NCl_2 (MC)	N···Cl	2.6023	0.0285	0.0933	0.0013	0.0220	−0.0207	MC
H_3NBr_2 (MC)	N···Br	2.5976	0.0341	0.0970	−0.0005	0.0248	−0.0253	MC
H_2SCl_2 (MC)	S···Cl	3.1558	0.0145	0.0464	0.0015	0.0101	−0.0087	MC
H_2SBr_2 (MC)	S···Br	3.0597	0.0219	0.0552	−0.0002	0.0140	−0.0142	MC
H_2SeCl_2 (MC)	Se···Cl	3.2117	0.0155	0.0440	0.0012	0.0098	−0.0086	MC
H_2SeBr_2 (MC)	Se···Br	3.1404	0.0217	0.0505	−0.0001	0.0128	−0.0129	MC
Cl_3^-[c]	Cl···Cl	2.2924	0.0858	0.0942	−0.0270	0.0506	−0.0776	X_3^-
Br_3^-[c]	Br···Br	2.5703	0.0641	0.0671	−0.0152	0.0320	−0.0472	X_3^-
$ClBrCl^-$	Cl···Br	2.4510	0.0753	0.0803	−0.0220	0.0421	−0.0641	X_3^-
$BrClBr^-$	Br···Cl	2.4086	0.0715	0.0794	−0.0183	0.0381	−0.0564	X_3^-
H_2SCl_2 (TBP)	S···Cl	2.2342	0.1031	0.0194	−0.0440	0.0488	−0.0928	TBP-ZX_2
H_2SBr_2 (TBP)	S···Br	2.4297	0.0823	0.0324	−0.0276	0.0357	−0.0634	TBP-ZX_2
H_2SeCl_2 (TBP)	Se···Cl	2.3337	0.0905	0.0259	−0.0380	0.0444	−0.0824	TBP-ZX_2
H_2SeBr_2 (TBP)	Se···Br	2.5253	0.0738	0.0293	−0.0233	0.0306	−0.0539	TBP-ZX_2
H_2SCl^+	S···Cl	1.9832	0.1666	−0.1309	−0.1033	0.0706	−0.1739	Cov-w
H_2SeBr^+	Se···Br	2.2778	0.1163	−0.0484	−0.0565	0.0444	−0.1009	Cov-w
H_2SCl_2 (MC)	Cl···Cl	2.0091	0.1538	−0.0230	−0.0836	0.0778	−0.1614	Cov-w
H_2SBr_2 (MC)	Br···Br	2.3198	0.1041	0.0100	−0.0417	0.0442	−0.0859	Cov-w
H_2SeCl_2 (MC)	Cl···Cl	2.0136	0.1525	−0.0196	−0.0823	0.0774	−0.1596	Cov-w
H_2SeBr_2 (MC)	Br···Br	2.3265	0.1028	0.0126	−0.0408	0.0439	−0.0847	Cov-w
Cl_2	Cl···Cl	1.9949	0.1581	−0.0347	−0.0880	0.0794	−0.1674	Cov-w
Br_2	Br···Br	2.2912	0.1093	−0.0004	−0.0460	0.0459	−0.0919	Cov-w
C_2H_6[b]	C···C	1.5230	0.2433	−0.6044	−0.2050	0.0539	−0.2589	Cov-s

[a] The MP2/6-311+G(2df,2p) method being employed except for Ar and Kr; the MP2/6-311G(2df,2p) method employed for Ar and Kr. [b] See also ref 17. [c] See also ref 24.

It is instructive to explain the outline of the AIM dual parameter analysis before the treatment of the interactions by this method. Trihalide ions (X_3^-: X = Cl and Br) are employed for the pre-explanation of the treatment, since X_3^- supply a suitable system for the calculations under the variously fixed r(X, X).

Survey of AIM Dual Parameter Analysis. Optimized structures of trihalide ions (Cl_3^- and Br_3^-) have $D_{\infty h}$ symmetry with $r_o(^1X, ^2X)$ ($=r_o$) = 2.292 and 2.570 Å, respectively (Table 1). They are further optimized under the fixed values of $r = r_o + 0.1n$ Å with $n = -5, -4, -3, -2, -1, (0), 1, 2, 3, 4, 5, 7, 9, 11, 13, 15, 25, 35, 45$.[46] The ions can be expressed by $^1X-^2X----^3X^-$ for $n < 0$ and $^1X^-----^2X-^3X$ for $n \gg 1$. The plots of $\Delta\rho_b(\boldsymbol{r}_c)$ and $H_b(\boldsymbol{r}_c)$ versus $r(^1X, ^2X)$ for Cl_3^- and Br_3^- (and F_3^-) are shown in Figure S1 of the SI. The plots of $H_b(\boldsymbol{r}_c)$ versus $\rho_b(\boldsymbol{r}_c)$ for Cl_3^- and Br_3^- (and F_3^-) are shown in Figure S2 of the SI.

Figure 1 shows the plots of $H_b(\boldsymbol{r}_c)$ versus $\Delta\rho_b(\boldsymbol{r}_c)$ for Cl_3^- and Br_3^-. Data corresponding to the optimized structures are shown by stars (★). While $\Delta\rho_b(\boldsymbol{r}_c)$ of Cl_3^- and Br_3^- are both positive, $H_b(\boldsymbol{r}_c)$ are both negative at r_o (Table 1). The origin of Figure 1 corresponds to $\Delta\rho_b(\boldsymbol{r}_c) = H_b(\boldsymbol{r}_c) = 0$ ($=\rho_b(\boldsymbol{r}_c)$), where the $^1X----^2X$ interactions in $^1X----^2X-^3X$ are extremely weak with very large $r(^1X, ^2X)$.

As shown in Figure 1, the plots of $H_b(\boldsymbol{r}_c)$ versus $\Delta\rho_b(\boldsymbol{r}_c)$ give helical figures for both Cl_3^- and Br_3^-. The plots start substantially from the origin ($\Delta\rho_b(\boldsymbol{r}_c) = H_b(\boldsymbol{r}_c) = 0$ ($=\rho_b(\boldsymbol{r}_c)$)). $H_b(\boldsymbol{r}_c)$ grow larger as the interactions become stronger and they reach maxima where the plots bend. Then $H_b(\boldsymbol{r}_c)$ decrease to negative via zero whereas $\Delta\rho_b(\boldsymbol{r}_c)$ become larger for a while. The second bending points in the plots appear at $\Delta\rho_b(\boldsymbol{r}_c)$ being maxima,

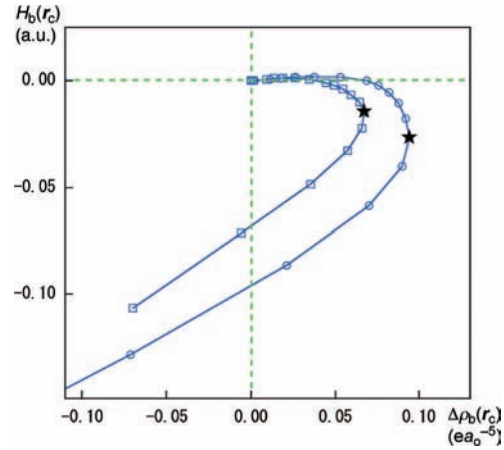

Figure 1. Plots of $H_b(\boldsymbol{r}_c)$ versus $\Delta\rho_b(\boldsymbol{r}_c)$ for Cl_3^- (○) and Br_3^- (□). Data corresponding to the optimized structures are shown by ★.

where $H_b(\boldsymbol{r}_c) < 0$ but $\Delta\rho_b(\boldsymbol{r}_c) > 0$. After the second bending, $\Delta\rho_b(\boldsymbol{r}_c)$ decrease to negative via zero, while $H_b(\boldsymbol{r}_c)$ decrease more and more. Both $H_b(\boldsymbol{r}_c)$ and $\Delta\rho_b(\boldsymbol{r}_c)$ are negative and decrease monotonically at the final stage of the plots. As a result, the plots turn to the right helical curves.

Why do the plots of $H_b(\boldsymbol{r}_c)$ versus $\Delta\rho_b(\boldsymbol{r}_c)$ curve helically? What mechanism causes such behavior? The next extension is to examine the weak to strong interactions by AIM dual parameter analysis.

AIM Dual Parameter Analysis of Weak to Strong Interactions. Figure 2 shows the plots of $H_b(\boldsymbol{r}_c)$ versus $\Delta\rho_b(\boldsymbol{r}_c)$ for weak to strong interactions in Scheme 1 and/or Table 1,

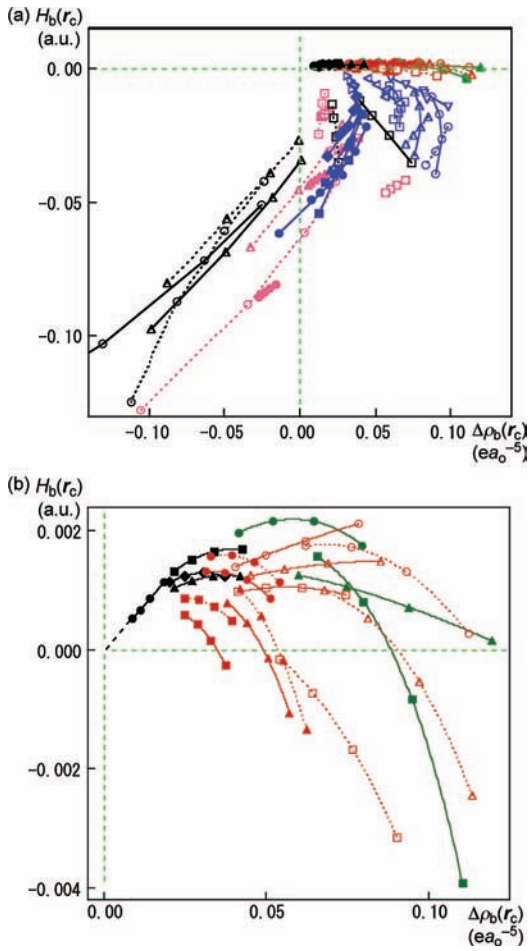

Figure 2. Plots of $H_b(r_c)$ versus $\Delta\rho_b(r_c)$ for weak to strong interactions; data obtained at $r_o - 0.1$, r_o, $r_o + 0.1$, and $r_o + 0.2$ Å are employed: (a) the whole picture of the plots and (b) the partial picture for vdW, HB, and MC.

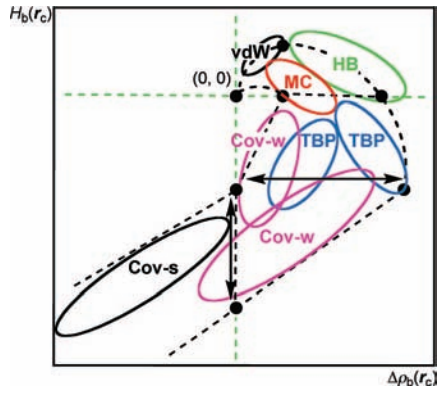

Figure 3. Characteristics for the plots of $H_b(r_c)$ versus $\Delta\rho_b(r_c)$.

employing the data calculated at $r = r_o + 0.1n$ Å ($n = -1$, (0), 1, and 2), where r_o are the optimized distances. Panels a and b of Figure 2 show the whole picture of the plots and the partial one for vdW, HB, and MC, respectively.

The plots show a helical figure as a whole, similarly to the case of Cl_3^- and Br_3^- (see Figure 1). The plots spread over a wider band around the mean helical curve, compared with the plots of $H_b(r_c)$ versus $\rho_b(r_c)$ (cf: Figure S2 in the SI). Data calculated at $r = r_o - 0.1$, $r_o + 0.1$, and $r_o + 0.2$ Å seem to behave similarly to those at $r = r_o$ in the plots. The Z--*--X interactions in H_2ZX_2 (TBP: Z = S and Se, X = Cl, Br, and I) are essentially separated from those in H_2ZX_2 (MC: Z = O, N, S, and Se, X = Cl, Br, and I) and from those in trihalide ions in the plots (Figure 2a). A plot gives the specific curvature for each, which must play an important role to understand and analyze the interactions in a unified way. Figure 3 illustrates schematically the characteristics observed in Figure 2. Table 2 summarizes the rough values for $\Delta\rho_b(r_c)$ and $H_b(r_c)$ in the interactions, together with $\rho_b(r_c)$, although some already have been pointed out.[38]

Data in the plots of $H_b(r_c)$ versus $\Delta\rho_b(r_c)$ for the interactions along with the mean helical line in Figure 2 appear in an order given by eq 4, where "<" shows the sequence of the appearance starting from near origin. The sequence is also confirmed in Figure 3 and Table 2.

$$\text{vdW} < \text{HB} \leq \text{CT-MC} < \text{CT-TBP (trihalide anion)} < \text{CT-TBP (chalcogenide dihalides)} < \text{Cov-bonds (weak)} < \text{Cov-bonds (strong)} \quad (4)$$

Weak to strong interactions are well understood and classified by the AIM dual parameter analysis through the plots of $H_b(r_c)$ versus $\Delta\rho_b(r_c)$, which show the helical behavior. Why do such behaviors appear in the plots? The reason is considered next.

Factors to Control the Helical Behavior. Factors to control the helical behavior will be clarified by decomposing $H_b(r_c)$ to $[H_b(r_c) - (1/2)V_b(r_c)]$ and $(1/2)V_b(r_c)$, where $[H_b(r_c) - (1/2)V_b(r_c)] = \hbar^2/8m\Delta\rho_b(r_c)$ (eq 2). They are plotted versus $\Delta\rho_b(r_c)$. Figure 4 shows the results. Panels a and b of Figure 4 construct Figure 2.

The plots of $[H_b(r_c) - (1/2)V_b(r_c)]$ versus $\Delta\rho_b(r_c)$ give a regular proportion with a correlation constant of 0.125 (=1/8 a.u. = $\hbar^2/8m$ a.u.; see eq 2)[47] (Figure 4a). On the other hand, the plots of $(1/2)V_b(r_c)$ versus $\Delta\rho_b(r_c)$ exhibit the helical character (Figure 4b). Apparently, the observed helical character in the plots of $H_b(r_c)$ versus $\Delta\rho_b(r_c)$ originates from the plot of $(1/2)V_b(r_c)$ versus $\Delta\rho_b(r_c)$.

What quadrant do the data for an interaction appear in? Requirements for a point to appear in a quadrant are examined. $H_b(r_c)$ (=$G_b(r_c) + V_b(r_c)$) is chosen as the y-axis and $\Delta\rho_b(r_c)$ is employed for the x axis where $(\hbar^2/8m)\Delta\rho_b(r_c) = G_b(r_c) + (1/2)V_b(r_c)$. Consequently, the boundary conditions at $y = 0$ and $x = 0$ are $G_b(r_c) = -V_b(r_c)$ and $G_b(r_c) = -(1/2)V_b(r_c)$, respectively. The requirements are clarified based on the boundary conditions. The requirements for a point to appear in the first quadrant ($\Delta\rho_b(r_c) > 0$ and $H_b(r_c) > 0$) are $-V_b(r_c) < G_b(r_c)$, those for the third ($\Delta\rho_b(r_c) < 0$ and $H_b(r_c) < 0$) and the forth ones ($\Delta\rho_b(r_c) > 0$ and $H_b(r_c) < 0$) are $G_b(r_c) < -(1/2)V_b(r_c)$ and $-(1/2)V_b(r_c) < G_b(r_c) < -V_b(r_c)$, respectively. There are no reasonable correlations for the second one ($\Delta\rho_b(r_c) < 0$ and $H_b(r_c) > 0$).[48] Therefore, no points appear in the second quadrant. Scheme 4 summarizes the results. The relative magnitudes of $G_b(r_c)$ versus $V_b(r_c)$ control the requirements. The requirements can be well recognized by the plots of $G_b(r_c)$ versus $V_b(r_c)$, which are shown in Figure S3 in the SI.

Meanings of the AIM Dual Parameter Analysis. The shared-shell (SS) signature is evidenced by a local concentration of $\rho_b(r_c)$ relative to the average distribution around BCP with $\Delta\rho_b(r_c) < 0$, whereas the closed-shell (CS) interactions exhibit a local depletion of $\rho_b(r_c)$ for $\Delta\rho_b(r_c) > 0$. The CS interactions at BCP are especially called *pure* CS interactions if $H_b(r_c) > 0$, since electrons at BCP are not stabilized under the conditions.[33a] The intermediate region between SS and pure CS, which belongs to CS, is related to the redistribution of $\rho_b(r_c)$ between those electronic states.[33a] Electrons at BCP are stabilized but not locally concentrated in this region, since $H_b(r_c) < 0$ but $\Delta\rho_b(r_c) > 0$. Scheme 5 summarizes the results.

TABLE 2: Typical Ranges of $\rho_b(r_c)$, $\Delta\rho_b(r_c)$, and $H_b(r_c)$ for Adducts and Molecules[a]

interaction	$\rho_b(r_c)$	$\Delta\rho_b(r_c)$	$H_b(r_c)$
vdW	$0.00 < \rho_b(r_c) < 0.01$	$0.00 < \Delta\rho_b(r_c) < 0.04$	$0.000 < H_b(r_c) < 0.002$
HB	$0.01 < \rho_b(r_c) < 0.04$	$0.04 < \Delta\rho_b(r_c) < 0.12$	$-0.004 < H_b(r_c) < 0.002$
CT-MC	$0.01 < \rho_b(r_c) < 0.03$	$0.02 < \Delta\rho_b(r_c) < 0.06$	$-0.001 < H_b(r_c) < 0.002$
CT-TBP	$0.03 < \rho_b(r_c) < 0.12$	$-0.01 < \Delta\rho_b(r_c) < 0.1$	$-0.06 < H_b(r_c) < -0.003$
Cov-w	$0.05 < \rho_b(r_c) < 0.17$	$-0.1 < \Delta\rho_b(r_c) < 0.07$	$-0.13 < H_b(r_c) < -0.03$

[a] $0.03 < \Delta\rho_b(r_c) < 0.1$ for trihalide ions and $-0.01 < \Delta\rho_b(r_c) < 0.04$ for H_2ZX_2 (TBP: Z = S and Se and X = Cl and Br).

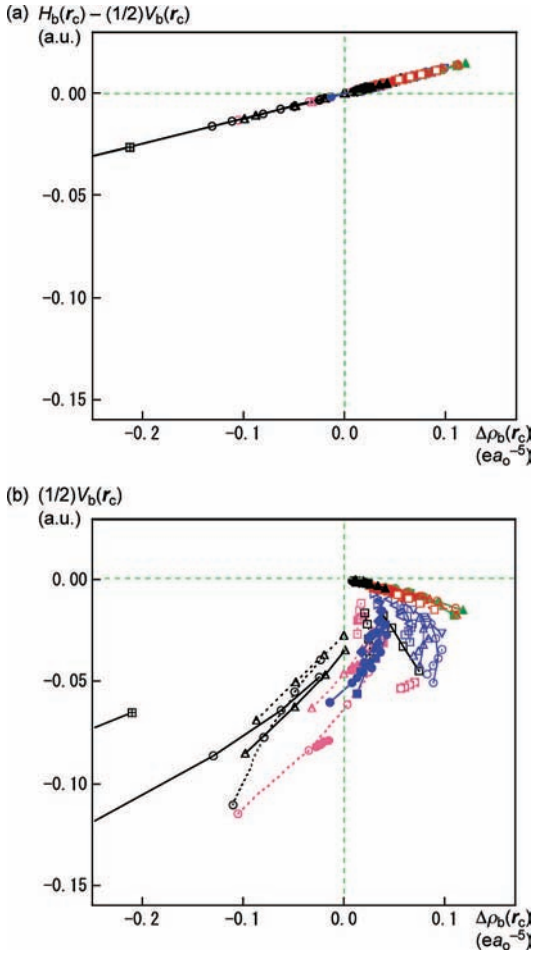

Figure 4. (a) Plots of $[H_b(r_c) - (1/2)V_b(r_c)]$ versus $\Delta\rho_b(r_c)$ and (b) plots of $(1/2)V_b(r_c)$ versus $\Delta\rho_b(r_c)$.

SCHEME 4: Requirements for the Data to Appear in a Certain Quadrant in the Plots of $H_b(r_c)$ versus $\Delta\rho_b(r_c)$

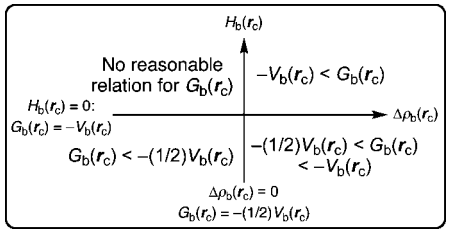

The helical nature of the interactions in the plots of $H_b(r_c)$ versus $\Delta\rho_b(r_c)$ helps us to understand the interactions in a unified way. The physical meanings of the plots proposed in this work become clear if one compares the results shown in Scheme 4 with those in Scheme 5. The SS, CS, and pure CS interactions are well correlated to the AIM dual parameter analysis, although we must be careful when the characteristic behaviors at the border area of the interactions are discussed.

SCHEME 5: The Nature of the Chemical Bonds and Interactions Classified by $H_b(r_c)$ and $\Delta\rho_b(r_c)$

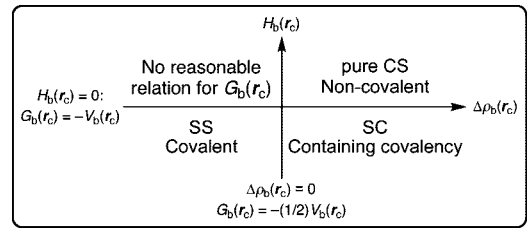

Conclusion

Plots of $H_b(r_c)$ versus $\Delta\rho_b(r_c)$ for weak to strong interactions construct a helical stream as a whole. The helical nature of the plots is controlled by the relative magnitudes between $G_b(r_c)$ and $V_b(r_c)$, where $G_b(r_c) + V_b(r_c) = H_b(r_c)$. Data in the plots start substantially from the origin ($\Delta\rho_b(r_c) = H_b(r_c) = 0$) and $H_b(r_c)$ grows larger as the interactions become stronger. They reach maxima where the plots bend. The second bending point of the mean line for the plots appears at $\Delta\rho_b(r_c)$ being maximum, where $H_b(r_c) < 0$ and $\Delta\rho_b(r_c) > 0$. After the second bending, $\Delta\rho_b(r_c)$ begins to decrease then becomes negative via zero, while $H_b(r_c)$ decreases more and more. Both $H_b(r_c)$ and $\Delta\rho_b(r_c)$ are negative at the final stage of the plots, which corresponds to the strong covalent interactions. The stream of data spreads over a relatively wide range around the mean helical curve. Consequently, data for weak interactions appear substantially separated in the treatment.

Requirements for a point to appear in the specified quadrant are clarified. Data will appear in the first quadrant ($\Delta\rho_b(r_c) > 0$ and $H_b(r_c) > 0$) when $-V_b(r_c) < G_b(r_c)$, they drop in the forth quadrant ($\rho_b(r_c) > 0$ and $H_b(r_c) < 0$) if $-(1/2)V_b(r_c) < G_b(r_c) < -V_b(r_c)$, as well as in the third quadrant ($\Delta\rho_b(r_c) < 0$ and $H_b(r_c) < 0$) if $G_b(r_c) < -(1/2)V_b(r_c)$. No points will appear in the second quadrant ($\Delta\rho_b(r_c) < 0$ and $H_b(r_c) < 0$), since no reasonable correlations are found for the second quadrant. The physical meanings of the plots proposed in this work are clarified. The curvature in the plot of $H_b(r_c)$ versus $\Delta\rho_b(r_c)$ for each species must be important when the interactions are analyzed, classified, and understood in a unified way.

Investigations for the applications of the proposed method are in progress. The results will be reported elsewhere.

Acknowledgment. This work was partially supported by a Grant-in-Aid for Scientific Research (Nos. 16550038, 19550041, and 20550042) from the Ministry of Education, Culture, Sports, Science, and Technology, Japan.

Supporting Information Available: AIM parameters for examined molecules and adducts; plots of $H_b(r_c)$ and $\Delta\rho_b(r_c)$ versus r(X, X) for X_3^- (X = F, Cl, and Br), plots of $H_b(r_c)$ versus $\Delta\rho_b(r_c)$ for X_3^- (X = F, Cl, and Br), plots of $G_b(r_c)$ versus $V_b(r_c)$ for examined molecules and adducts, optimized structures given by Cartesian coordinates for examined molecules and

adducts (PDF). This material is available free of charge via the Internet at http://pubs.acs.org.

References and Notes

(1) (a) *Molecular Interactions. From van der Waals to Strongly Bound Complexes*: Scheiner, S., Ed.; Wiley: New York,1997. (b) Asmus, K. D. *Acc. Chem. Res.* **1979**, *12*, 436–442. (c) Musker, W. K. *Acc. Chem. Res.* **1980**, *13*, 200–206. (d) Kucsman, A.; Kapovits, I. Non-Bonded Sulfur-Oxygen Interaction in Organic Sulfur Compounds. In *Organic Sulfur Compounds in Organic Sulfur Chemistry: Theoretical and Experimental Advances*; Bernardi, F., Csizmadia, I. G., Mangini, A., Eds.; Elsevier: Amsterdam, The Netherlands,1985; Chapter 4.

(2) (a) *Chemistry of Hypervalent Compounds*; Akiba, K.-y., Ed.; Wiley-VCH: New York,1999. (b) Nakanishi, W. Hypervalent Chalcogen Compounds. In *Handbook of Chalcogen Chemistry: New Perspectives in Sulfur, Selenium and Tellurium*; Devillanova, F. A., Ed.; Royal Society of Chemistry: Cambridge, UK, 2006; Chapter 10.3, pp 644−668.

(3) Glusker, J. P. Directional aspects of intermolecular interactions. In *Topics in Current Chemistry, Design of Organic Solids*; Weber, E., Ed.; Springer Verlag: Berlin, Heidelberg, Germany, 1998; Vol. 198, pp 1−56.

(4) Iwaoka, M.; Tomoda, S. *J. Am. Chem. Soc.* **1996**, *118*, 8077–8084. Iwaoka, M.; Takemoto, S.; Tomoda, S. *J. Am. Chem. Soc.* **2002**, *124*, 10613–10620. Iwaoka, M.; Takemoto, S.; Okada, M.; Tomoda, S. *Chem. Lett.* **2001**, *30*, 132–133.

(5) (a) Nakanishi, W. *Chem. Lett.* **1993**, 2121–2122. (b) Nakanishi, W.; Hayashi, S.; Toyota, S. *Chem. Commun.* **1996**, 371–372. (c) Nakanishi, W.; Hayashi, S.; Yamaguchi, H. *Chem. Lett.* **1996**, 947–948. (d) Nakanishi, W.; Hayashi, S.; Sakaue, A.; Ono, G.; Kawada, Y. *J. Am. Chem. Soc.* **1998**, *120*, 3635–3640. (e) Nakanishi, W.; Hayashi, S.; Toyota, S. *J. Org. Chem.* **1998**, *63*, 8790–8800. (f) Hayashi, S.; Nakanishi, W. *J. Org. Chem.* **1999**, *64*, 6688–6696. (g) Nakanishi, W.; Hayashi, S.; Uehara, T. *J. Phys. Chem. A* **1999**, *103*, 9906–9912. (h) Nakanishi, W.; Hayashi, S. *J. Org. Chem.* **2002**, *67*, 38–48. (i) Hayashi, S.; Wada, H.; Ueno, T.; Nakanishi, W. *J. Org. Chem.* **2006**, *71*, 5574–5585. (j) Nakanishi, W.; Hayashi, S.; Kihara, H. *J. Org. Chem.* **1999**, *64*, 2630–2637. (k) Nakanishi, W.; Hayashi, S.; Uehara, T. *Eur. J. Org. Chem.* **2001**, 3933–3943.

(6) Rosenfield, R. E., Jr.; Parthasarathy, R.; Dunitz, J. D. *J. Am. Chem. Soc.* **1977**, *99*, 4860–4862.

(7) *The Weak Hydrogen Bond in Structural Chemistry and Biology; International Union of Crystallography Monographs on Crystallography*; Desiraju, G. R., Steiner, T., Eds.;Oxford University Press: New York, 1999. *Crystal Design: Structure and Function (Perspectives in Supramolecular Chemistry, Vol. 6*; Desiraju, G. R., Ed.; John Wiley & Sons: New York, 2003.

(8) Steiner, T. Angew. Chem. 2002, 114, 50−80; Angew. Chem., Int. Ed. **2002**, *41*, 4876.

(9) (a) Bleiholder, C.; Werz, D. B.; Köppel, H.; Gleiter, R. *J. Am. Chem. Soc.* **2006**, *128*, 2666–2674. (b) Bleiholder, C.; Gleiter, R.; Werz, D. B.; Köppel, H. *Inorg. Chem.* **2007**, *46*, 2249–2260.

(10) Rêthorê, C.; Madalan, A.; Fourmiguê, M.; Canadell, E.; Lopes, E. B.; Almeida, M.; Clêrac, R.; Avarvari, N. *New J. Chem.* **2007**, *31*, 1468–1483.

(11) Werz, D. B.; Gleiter, R.; Rominger, F. *J. Am. Chem. Soc.* **2002**, *124*, 10638–10639. Gleiter, R.; Werz, D. B.; Rausch, B. J. *Chem. Eur. J.* **2003**, *9*, 2676–2683. Werz, D. B.; Gleiter, R.; Rominger, F. *J. Org. Chem.* **2004**, *69*, 2945–2952. Gleiter, R.; Werz, D. B. *Chem. Lett.* **2005**, *34*, 126–131. Werz, D. B.; Rausch, B. J.; Gleiter, R. *Tetrahedron Lett.* **2002**, *43*, 5767–5769.

(12) Suzuki, T.; Fujii, H.; Yamashita, Y.; Kabuto, C.; Tanaka, S.; Harasawa, M.; Mukai, T.; Miyashi, T. *J. Am. Chem. Soc.* **1992**, *114*, 3034–3043. Turbiez, M.; Frêre, P.; Allain, M.; Videlot, C.; Ackermann, J.; Roncali, J. *Chem. Eur. J.* **2005**, *11*, 3742–3752. Cozzolino, A. F.; Vargas-Baca, I.; Mansour, S.; Mahmoudkhani, A. H. *J. Am. Chem. Soc.* **2005**, *127*, 3184–3190.

(13) Lippolis, V.; Isaia, F. Charge-Transfer (C.-T.) Adducts and Related Compounds. In *Handbook of Chalcogen Chemistry: New Perspectives in Sulfur, Selenium and Tellurium*; Devillanova,F. A., Ed.; Royal Society of Chemistry: Cambridge, UK, 2006; Chapter 8.2, pp 477−499. Rêthorê, C.; Fourmiguê, M.; Avarvari, N. *Chem. Commun.* **2004**, 1384−1385. Rêthorê, C.; Fourmiguê, M.; Avarvari, N. *Tetrahedron* **2005**, *61*, 10935–10942. Rêthorê, C.; Avarvari, N.; Canadell, E.; Auban-Senzier, P.; Fourmiguê, M. *J. Am. Chem. Soc.* **2005**, *127*, 5748–5749.

(14) Desiraju, G. R. *Angew. Chem.* **1995**, *107*, 2541–2558. Desiraju, G. R. Angew. Chem., Int. Ed. Engl. **1995**, *34*, 2311−2327. *Supramolecular Chemistry*; Steed, J. W., Atwood, J. L., Eds.; John Wiley & Sons: New York, 2000. *Supramolecular Chemistry: Concepts and Perspectives*; Lehn,J.-M., Ed.; Wiley-VCH: Weinheim, Germany, 1995. *Principles and Methods in Supramolecular Chemistry*; Schneider, H.-J., Yatsimirsky, A. K., Eds.;John Wiley & Sons: New York, 2000. Guru Row, T. N.; Parthasarathy, R. *J. Am. Chem. Soc.* **1981**, *103*, 477–479.

(15) Burling, F. T.; Goldstein, B. M. *J. Am. Chem. Soc.* **1992**, *114*, 2313–2320. Nagao, Y.; Hirata, T.; Goto, S.; Sano, S.; Kakehi, A.; Iizuka, K.; Shiro, M. *J. Am. Chem. Soc.* **1998**, *120*, 3104–3110. Wu, S.; Greer, A. *J. Org. Chem.* **2000**, *65*, 4883–4887. Nagao, Y.; Iimori, H.; Goto, S.; Hirata, T.; Sano, S.; Chuman, H.; Shiro, M. *Tetrahedron Lett.* **2002**, *43*, 1709–1712. Meyer, E.; Joussef, A. C.; Gallardo, H.; Bortoluzzi, A. J.; Longo, R. L. *Tetrahedron* **2003**, *59*, 10187–10193. Nagao, Y.; Honjo, T.; Iimori, H.; Goto, S.; Sano, S.; Shiro, M.; Yamaguchi, K.; Sei, Y. *Tetrahedron Lett.* **2004**, *45*, 8757–8761.

(16) Taylor, J. C.; Markham, G. D. *J. Biol. Chem.* **1999**, *274*, 32909–32914. Brandt, W.; Golbraikh, A.; Täger, M.; Lendeckel, U. *Eur. J. Biochem.* **1999**, *261*, 89–97.

(17) *Atoms in Molecules. A Quantum Theory*; Bader, R. F. W., Ed.; Oxford University Press: Oxford, UK, 1990.

(18) Matta, C. F.; Boyd, R. J. An Introduction to the Quantum Theory of Atoms in Molecules. In *The Quantum Theory of Atoms in Molecules: From Solid State to DNA and Drug Design*; Matta, C. F., Boyd, R. J., Eds.; Wiley-VCH: Weinheim, Germany, 2007; Chapter 1.

(19) (a) Bader, R. F. W.; Slee, T. S.; Cremer, D.; Kraka, E. *J. Am. Chem. Soc.* **1983**, *105*, 5061–5068. (b) Bader, R. F. W. *Chem. Res.* **1991**, *91*, 893–926. (c) Bader, R. F. W. *J. Phys. Chem. A* **1998**, *102*, 7314–7323. (d) Biegler-König, F.; Bader, R. F. W.; Tang, T. H. *J. Comput. Chem.* **1982**, *3*, 317–328. (e) Bader, R. F. W. *Acc. Chem. Res.* **1985**, *18*, 9–15. (f) Tang, T. H.; Bader, R. F. W.; MacDougall, P. *Inorg. Chem.* **1985**, *24*, 2047–2053. (g) Biegler-König, F.; Schönbohm, J.; Bayles, D. *J. Comput. Chem.* **2001**, *22*, 545–559. (h) Biegler-König, F.; Schönbohm, J. *J. Comput. Chem.* **2002**, *23*, 1489–1494.

(20) Molina, J.; Dobado, J. A. *Theor. Chem. Acc.* **2001**, *105*, 328–337.

(21) Dobado, J. A.; Martinez-Garcia, H.; Molina, J.; Sundberg, M. R. *J. Am. Chem. Soc.* **2000**, *122*, 1144–1149.

(22) Yamashita, M.; Yamamoto, Y.; Akiba, K.-Y.; Hashizume, D.; Iwasaki, F.; Takagi, N.; Nagase, S. *J. Am. Chem. Soc.* **2005**, *127*, 4354–4371. Yamamoto, Y.; Akiba, K.-Y. *J. Synth. Org. Chem. Jpn.* **2004**, *62*, 1128–1137.

(23) Ignatov, S. K.; Rees, N. H.; Tyrrell, B. R.; Dubberley, S. R.; Razuvaev, A. G.; Mountford, P.; Nikonov, G. I. *Chem. Eur. J.* **2004**, *10*, 4991–4999.

(24) Muchall, H. M. *ARKIVOC* **2001**, *7*, 82–86.

(25) Tripathi, S. K.; Patel, U.; Roy, D.; Sunoj, R. B.; Singh, H. B.; Wolmershäuser, G.; Butcher, R. J. *J. Org. Chem.* **2005**, *70*, 9237–9247.

(26) Boyd, R. J.; Choi, S. C. *Chem. Phys. Lett.* **1986**, *129*, 62–65.

(27) Carroll, M. T.; Bader, R. F. W. *Mol. Phys.* **1988**, *65*, 695–722.

(28) Espinosa, E.; Molins, E.; Lecomte, C. *Chem. Phys. Lett.* **1998**, *285*, 170–173.

(29) Grabowski, S. J. *J. Phys. Chem. A* **2001**, *105*, 10739–10746.

(30) Domagala, M.; Grabowski, S.; Urbaniak, K.; Mloston, G. *J. Phys. Chem. A* **2003**, *107*, 2730–2736.

(31) Grabowski, S.; Sokalski, W. A.; Leszczynski, J. *J. Phys. Chem. A* **2005**, *109*, 4331–4341.

(32) Domagala, M.; Grabowski, S. *J. Phys. Chem. A* **2005**, *109*, 5683–5688.

(33) (a) Espinosa, E.; Alkorta, I.; Elguero, J.; Molins, E. *J. Chem. Phys.* **2002**, *117*, 5529–5542. (b) Rozas, I.; Alkorta, I.; Elguero, J. *J. Am. Chem. Soc.* **2000**, *122*, 11154–11161.

(34) For the linear alignment of five C_2Z_2O atoms in 1,8-(p-$YC_6H_4Z)_2$-$C_{14}H_6O_2$ and 9-MeO-1,8-(p-$YC_6H_4Z)_2C_{14}H_7$ (Z = S and Se)[48] see: Nakanishi, W.; Hayashi, S.; Itoh, N. *Chem. Commun* **2003**, *12*, 4–125. Nakanishi, W.; Hayashi, S.; Itoh, N. *J. Org. Chem.* **2004**, *69*, 1676–1684. Nakanishi, W.; Hayashi, S.; Furuta, T.; Itoh, N.; Nishina, Y.; Yamashita, M.; Yamamoto, Y. *Phosphorus, Sulfur, Silicon* **2005**, *180*, 1351–1355.

(35) Nakanishi, W.; Nakamoto, T.; Hayashi, S.; Sasamori, T.; Tokitoh, N. *Chem. Eur. J.* **2007**, *13*, 255–268.

(36) For hydrogen bonds see: Espinosa, E.; Molins, E.; Lecomte, C. *Chem. Phys. Lett.* **1998**, *285*, 170–173. Espinosa, E.; Souhassou, M.; Lachekar, H.; Lecomte, C. *Acta Crystallogr. B* **1999**, *55*, 563–572. Espinosa, E.; Lecomte, C.; Molins, E. *Chem. Phys. Lett.* **1999**, *300*, 745–748. Espinosa, E.; Alkorta, I.; Rozas, I.; Elguero, J.; Molins, E. *Chem. Phys. Lett.* **2001**, *336*, 457–461. Gatti, C.; Bertini, L. *Acta Crystallogr. A* **2004**, *60*, 438–449.

(37) For van der Waals interactions, see also: Dessent, C. E. H.; Müller-Dethlefs, K. *Chem. Rev.* **2000**, *100*, 3999−4021. Wormer, P. E. S.; van der Avoird, A. *Chem. Rev.* **2000**, *100*, 4109–4143.

(38) Dominiak, P. M.; Makal, A.; Mallinson, P. R.; Trzcinska, K.; Eilmes, J.; Grech, E.; Chruszcz, M.; Minor, W.; Woźniak, K. *Chem. Eur. J.* **2006**, *12*, 1941–1949.

(39) Frisch, M. J.; et al. *Gaussian 03*, Revision D.02; Gaussian, Inc., Wallingford, CT, 2004.

(40) Møller, C.; Plesset, M. S. *Phys. Rev.* **1934**, *46*, 618–622. Gauss, J. *J. Chem. Phys.* **1993**, *99*, 3629–3643. Gauss, J. *Ber. Bunsenges, Phys. Chem.* **1995**, *99*, 1001–1008.

(41) The molecular graph is known as the collection of bond paths linking the nuclei of bonded atoms with the associated critical points in the equilibrium geometry. The molecular graph provides an unambiguous definition of the "molecular structure" and can thus be used to locate changes in the structure along a reaction path.[17,18]

(42) In a non-equilibrium geometry contained in this treatment, lines of maximum electron density linking the nuclei are known as "atomic interaction lines", because these may or may not persist when the geometry is energy-minimized, i.e. optimized.[17,18] However, the trends could be discussed as the extension of those for the optimized structures in our treatment, since the geometries converge to the optimized structures when started from the given non-equilibrium ones.

(43) The bond orders become 1.47 and 0.46 times larger than the initial value if the bond lengths are calculated at 0.1 Å shorter and 0.2 Å longer from the initial length, respectively.[49] The change seems to affect not so much on our discussion to classify the weak interactions.

(44) Regardless of the definition shown in ref 42 we will call the AIM parameters at $r_o - 0.1 < r < r_o + 0.2$ Å similarly to the case of the equilibrium geometry here.

(45) The AIM 2000 program (Version 2.0) is employed to analyze and visualize atoms-in-molecules: Biegler-König, F. J. *Comput. Chem* **2000**, *21*, 1040–1048; see also ref 19g.

(46) This is the extreme case of $n = -1$, (0), 1, and 2. However, geometries converge again to the optimized ones when started from the given non-equilibrium ones, as discussed in the text. See also refs 42 and 44.

(47) Equations R1 and R2 explain the relationship in Figure 4a, where $H_b(\boldsymbol{r}_c) < (\hbar^2/8m)\Delta\rho_b(\boldsymbol{r}_c)$, since $V_b(\boldsymbol{r}_c) < 0$. This relationship is important in the requirement for the first quadrant,[50] which is given by eq R3.

$$[H_b(\boldsymbol{r}_c) - (1/2)V_b(\boldsymbol{r}_c)] = (\hbar^2/8m)\Delta\rho_b(\boldsymbol{r}_c) \quad \text{(R1)}$$

$$(1/2)V_b(\boldsymbol{r}_c) = H_b(\boldsymbol{r}_c) - (\hbar^2/8m)\Delta\rho_b(\boldsymbol{r}_c) < 0 \quad \text{(R2)}$$

$$0 < H_b(\boldsymbol{r}_c) < (\hbar^2/8m)\Delta\rho_b(\boldsymbol{r}_c) \quad \text{(R3)}$$

(48) The nonbonded Z---O distances are shorter than the sum of van der Waals radii. For the van der Waals radii see: Bondi, A. *J. Phys. Chem.* **1964**, *68*, 441–451.

(49) Pauling,L. *The Nature of the Chemical Bond*, 3rd ed.; Cornell University Press:Ithaca, NY, 1960; Chapter 7. Pauling, L. *J. Am. Chem. Soc.* **1947**, *69*, 542–553.

(50) The requirements given by $G_b(\boldsymbol{r}_c)$ and $V_b(\boldsymbol{r}_c)$ can also be represented employing $H_b(\boldsymbol{r}_c)$ and $V_b(\boldsymbol{r}_c)$. The requirements for the points to appear in the first, forth, and third quadrants are $0 < H_b(\boldsymbol{r}_c)$, $H_b(\boldsymbol{r}_c) < (1/2)V_b(\boldsymbol{r}_c)$, and $(1/2)V_b(\boldsymbol{r}_c) < H_b(\boldsymbol{r}_c) < 0$, respectively.

JP8054763